Received: 24 April 2021 | Revised: 28 July 2021 | Accepted: 17 August 2021

DOI: 10.1002/jemt.23919

RESEARCH ARTICLE

MICROSCOPY RESEARCH & TECHNIQUE WILEY

Mechanical test and friction-mapping on recycled polypropylene beads using atomic force microscopy

Mert Muhammed Koç[1] | Mustafa Oguzhan Caglayan[1,2]

[1]Faculty of Engineering, Department of Nanotechnology, Sivas Cumhuriyet University, Sivas, Turkey

[2]Faculty of Engineering, Department of Bioengineering, Bilecik Şeyh Edebali University, Bilecik, Turkey

Correspondence
Mustafa Oguzhan Caglayan, Sivas Cumhuriyet University, Faculty of Engineering, Nanotechnology Department, Sivas, Turkey.
Email: oguzhan.caglayan@bilecik.edu.tr

Funding information
Sivas Cumhuriyet Üniversitesi BAP, Grant/Award Number: M589

Review Editor: Alberto Diaspro

Abstract

Mechanical tests at sub-micron scales using force microscopy are often used for the characterization of materials. Here we report the mechanical, tribologic, and morphological characterization of recycled polypropylene beads using force spectroscopy and lateral-force microscopy. The compression-elastic moduli calculated using the Hertzian model for polypropylene beads was between 0.448 ± 0.010 and 1.044 ± 0.057 GPa. The grain size analysis revealed a significant correlation between the grain size and measured compression-elastic moduli. Friction-maps of recycled polypropylene beads obtained using lateral-force microscopy were also reported for 25 μm^2 scanning areas.

KEYWORDS
atomic force microscopy, elastic moduli, force spectroscopy, lateral force microscopy, nanoindentation, tribology

1 | INTRODUCTION

Mechanical tests, where important information about the structure and applicability of materials can be obtained, are very important in material characterization (Griepentrog, Krämer, & Cappella, 2013). There are several well-established techniques such as tensile testing and hardness testing, which provide reliable and comparable results on a macroscale and microscale (Narayanan, 1995; Vincent & Ramesh, 2015). However, macro-mechanics techniques can only be applied to homogeneous and large test samples. Mechanical test results obtained with traditional methods on macro and micro scales are not always valid on a nanoscale. For example, since a semi-crystalline material is composed of crystalline and amorphous regions with different mechanical properties on a nanoscale, more detailed information about the material can be obtained when its characterization is also performed on a nanoscale (Wang et al., 2015).

Developed to characterize the mechanical properties of non-homogeneous, or nanostructured materials at the nanoscale (Wornyo, Gall, Yang, & King, 2007), the nanoindentation technique has been widely used for the measurement of the material properties of polymers (Dominguez et al., 2012; Salerno, Dante, Patra, & Diaspro, 2010; Samadi-Dooki, Malekmotiei, & Voyiadjis, 2016), ceramics (Gao & Mäder, 2002), biological samples (Chen, Cui, & Chen, 2021; X. Li & Guo, 2019; Oyen, 2015; Sarialioglu Gungor & Donmez, 2021; Yang et al., 2019; Zheng, Guo, Li, & Ma, 2019), metallic alloys (L. Li, Guo, Xu, Li, & Han, 2017; X. Zhou, Jiang, Wang, & Yu, 2008), natural products (Kawasaki et al., 2017; Torres-Torres, Torres, & García-García, 2019), and composites (Nagasaki, Ishikawa, Ito, Saito, & Iijima, 2021; Young, Crocker, Broughton, Ogin, & Smith, 2013). Following the use of the method proposed by Oliver and Pharr (Oliver, 1992) for viscoelastic behavior, nanoindentation tests have been applied for the mechanical tests and characterization of single fibers (Wang et al., 2014; Yu, Wang, Lu, Tian, & Lin, 2014), polymer thin-films (Ago, Jakes, & Rojas, 2013; Francius et al., 2006; Morozov, 2021; Park, Frihart, Yu, & Singh, 2013; Vlad-Cristea, Riedl, Blanchet, & Jimenez-Pique, 2012), and multi-phase composite materials (Hardiman, Vaughan, & McCarthy, 2015; Lee, Wang, Pharr, & Xu, 2007; Loubet, Oliver, & Lucas, 2000; Rodríguez, Garrido-Maneiro, Poza, & Gómez-del Río, 2006). Properties such as interfacial adhesion strength and scratch resistance in polymer blends and films were also determined by nanoindentation and scratching tests (Davies et al., 2009; Mallikarjunachari & Ghosh, 2016; Wood et al., 2015).

The atomic force microscope (AFM) is one of delicate, high-resolution equipment that can be used for nanoindentation purposes

since its tip position can be controlled very precisely using piezoelectric actuators (Hoffmann et al., 2007) (Cappella & Silbernagl, 2008). Moreover, since the tip interacts with the sample surface according to the attractive and repulsive forces such as van der Waals, electrostatic and capillary forces, additional information on the surface interaction can be obtained using the cantilever position by a series of photodiodes. Using the cantilever spring constant and proposed calibration methods, the cantilever position is converted to quantitative force data obtained for either horizontal and lateral directions (Sader, Chon, & Mulvaney, 1999) (Figure 1a). There are various methods have been proposed for material characterization using AFM such as phase-spectroscopy (Jandt, 1998), lateral-force microscopy (Kotomin, Chang, Sancaktar, & Yarikov, 2014), and force spectroscopy (Barone et al., 2010; Cappella & Silbernagl, 2008). In the phase spectroscopy, the elastic modulus (Magonov, Elings, & Whangbo, 1997) and viscoelastic properties (García & Pérez, 2002) of the materials can be determined using the phase shift of natural oscillation frequency of the cantilever that interacted with the sample surface (Godehardt et al., 2004). Another AFM technique that is also used in this study is lateral-force microscopy, where tribological properties of coatings and microparticles can be obtained with a high resolution (Oliver & Pharr, 2011). Torsional deformation due to lateral forces applied to the AFM tip is measured in lateral force microscopy (Figure 1b). Elastic forces acting on this deformation enable the examination of the tribological properties of the materials depending on the friction and surface shapes (Song et al., 2012). More often, AFM is used for the determination of the elastic modulus utilizing nanoindentation tests (Kim, Yeon, Jeon, Kim, & Kim, 2003). Force spectroscopy is used for obtaining the force–distance curve that expresses the result of surface deformation and interactions as the distance change in the vertical scanner position for a single location in the sample (Cappella & Dietler, 1999) (Frisbie, Rozsnyai, Noy, Wrighton, & Lieber, 1994)

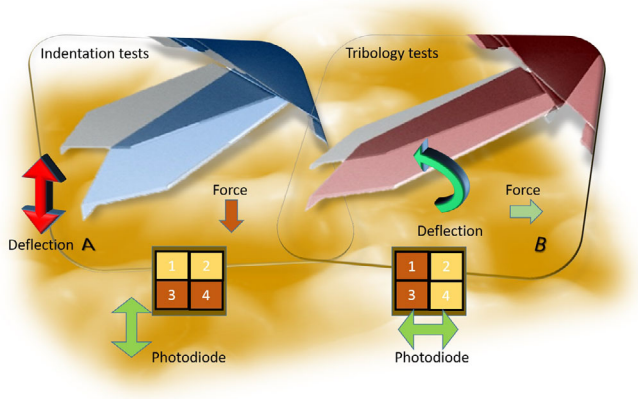

FIGURE 1 (a) The principle of measurement with vertical deflection used in indentation tests (normal force, the difference between 1–2 and 3–4 photodiodes is used for measurement), (b) torsional deflection measurement principle used in tribology experiments with lateral-force microscopy (lateral-force, the difference between 1–3 and 2–4 photodiodes is used for measurement)

(Withers & Aston, 2006). Elastic modulus and stiffness of the material can be calculated from force spectroscopy data using mechanical models such as the Hertz model (and Johnson–Kendall–Roberts (JKR) and Derjaguin–Muller–Toporov (DMT) models) (Benitez & Tocaherrera, 2014; Cappella & Silbernagl, 2008) or Oliver–Pharr model (Chakraborty, Sinha, Mukherjee, Ray, & Protim Chattopadhyay, 2013; Jin et al., 2015).

However, erroneous results may be obtained in the determination of the mechanical properties of polymers using nanoindentation due to substrate effects (Pelegri & Huang, 2008), surface effects (Zhang & Xu, 2011), and the pile-up behavior of polymers (Zhou & Komvopoulos, 2006). The elastic modulus, which is determined especially by using traditional macroscale mechanical tests, is generally smaller than the elastic modulus obtained by nanoindentation (Hardiman, Vaughan, & McCarthy, 2016). By different researchers, this has been linked to hydrostatic stress, pile-up behavior, or the viscoelastic behavior of polymer material (Cappella & Dietler, 1999; Greenwood & Johnson, 2006; Jin et al., 2015; King, Klimek, Miskioglu, & Odegard, 2013). One of the major problems with nanoindentation measurements with AFM is also the difficulty in determining the exact shape and size of the AFM tips (Butt, Cappella, & Kappl, 2005). Failure to accurately predict the actual contact area generally results in higher estimated elastic modulus values (Cao et al., 2006) (Bolshakov & Pharr, 2011).

It may be beneficial to use low loading rates and the depth of indentation to avoid the viscoelastic response of the material (Karapanagiotis, Evans, & Gerberich, 2002). Although it is difficult to say that complex polymeric materials do not have plasticity and viscoelasticity during the indentation process, it is generally accepted to use the rate of penetration versus the penetration depth as the representative stress rate (Ogasawara, Chiba, & Chen, 2005). There are additional features such as speed and force limit, ramping, and hold functions in modern AFM nanoindentation modes to overcome time-dependent deviations (VanLandingham, 2018). Usually, the interaction between the tip and the polymer for small forces immediately after contact is not significantly affected by adhesion, plastic deformations, and time-dependent phenomena. In this case, only elastic deformations are present. For this reason, studies conducted in the range in which the Hertz theory can be used instead of Oliver and Pharr's theory can aid to avoid problems arising from time-dependent phenomena such as adhesion, plastic deformations, and viscoelasticity (Oliver, 1992). Previous studies have reported the effectiveness of elastic models such as Hertz, DMT, and JKR models in measuring the elastic modulus of polymers at shallow indentation depths since the elastic response comes from the indentation zone and the base material (Greenwood & Johnson, 2006; Withers & Aston, 2006).

In this study, mechanical characterizations were carried out using polypropylene masterbatches containing different pigments obtained from the recycling facility. With the direct use of polymer beads, surface roughness analysis, grain analysis, and nanoindentation tests were carried out. Only the compression-elastic modulus was calculated by ensuring that the nanoindentation tests remain at only elastic deformation at constant indentation rates and depths. Also, using

calibrated AFM tip, interactions between the SiC probe and polymer beads were determined by lateral-force microscopy. The data obtained as a result of the tribology tests were used to obtain friction maps. To the best of our knowledge, this study is the first to perform nanoindentation tests to obtain compression–elastic modulus using recycled PP beads, and friction maps were also reported.

2 | MATERIALS AND METHODS

2.1 | General

In this study, topographic and mechanical property analysis of the material was carried out using the Park System XE-100 AFM device (Suwon, Korea). In the AFM device, measurements using a 650 nm laser diode can be performed at 4,096 × 4,096-pixel maximum resolution. NSC 36 probes (Suwon, Korea, 1 μm × 32.5 μm × 90 μm, maximum 9 N/m) supplied from the same production batch were used for measurements in the device equipped with ×780 inverted microscope.

Polypropylene (PP) beads without additives other than pigment obtained from different batches were used and named as P (1–7) depending on their density. The polymer beads with an average diameter of 0.8 cm were fixed on the glass slide and analyzed. All PP beads were washed with water and ethyl alcohol only before analysis and dried. Surface characterization was carried out in contact mode and surface roughness analysis was performed from topography data obtained. To meet the evaluation requirements in non-uniform samples, the analysis was performed in 10 different points in areas with 45 μm × 45 μm to 1 μm × 1 μm area using 5 randomly selected particle samples. In the topographic analysis, scanning speed was kept constant at 1 Hz. The surface particle structure was statistically evaluated using the built-in software of the device. Also, the surface roughness was calculated based on the entire scanning area.

The mechanical properties of polymer beads were determined by force spectroscopy (FS) using the nanoindentation method. The potential effect of viscoelastic properties on the experimental results in all samples was minimized by keeping the approach and retraction rates constant in the indentation process. In the test sample, indentation experiments were carried out in an area of 5 μm × 5 μm at 10 randomly selected points. During the indentation tests, the rate was set at 0.3 μm/s in both directions. The maximum loading was also set by the device as the value determined by the AFM device in accordance with the tip used. For each bead, 5 different areas were selected for indentation. The indentation was performed in 5 randomly selected samples for each different polymer set. Elastic behavior, if any, and plastic deformation were observed by obtaining *F–z* curves. Compression- elastic moduli (*E*) of the materials were calculated using the *F–z* curves by applying the Hertzian model where a built-in function is available in the software (Hertz, 1882). The Bilodeau model, which provides an approach to the application of the Hertz model to pyramid-shaped indentation tips, is more suitable for the tips used in this study (Bilodeau, 1992). There are some approaches of the Hertzian model, such as the assumption that there is no adhesion during contact (Weber, Iturri, Benitez, & Toca-Herrera, 2019). For this reason, it is important to choose the appropriate one in model selection (Cárdenas-Pérez et al., 2019). It was aimed, in this study, to reduce the limitations caused by contact mechanics by limiting the indentation depth and keeping the approach rate constant.

2.2 | Basic approaches used in the characterization

In this study, the FS module of the AFM device and built-in software connected to this module was used. In the nanoindentation process, the maximum load and indentation speed was set on the module. In FS mode, the AFM tip can exert vertical forces from several pN to μN ranges. During this process, the AFM tip is pressed from the surface of the sample at a certain distance, after the interaction, the AFM tip is brought back to its starting position. The data obtained is the force curve and enables the elastic and plastic properties of the sample to be determined. In this study, indentation was performed only in the elastic deformation region. The elastic region was determined by using the *F–z* curves obtained as a result of the indentation process as the linear region in the curves. Considering the force applied in this region (nN) and displacement data (nm), compression-elastic modulus (*E*) was calculated by the Hertzian model using the applied force (*F*, nN), Poisson ratio (ϑ, 0.45) for the material, typical half-peak angle of the AFM tip (α, 20°), and depth of indentation (δ) (Cappella & Silbernagl, 2008). Calculations were performed directly on the device's software called force spectroscopy, using the specifications of the indentation AFM tip declared by the manufacturer. Also, the shape of the AFM tip was estimated and re-checked using calibration patterns and modeling according to the method reported by Bhushan et al. (Bhushan & Kwak, 2007).

Lateral-force microscopy (LFM) analyzes on the Si (100) substrate were carried out with the AFM probe using SiC tip. LFM analyzes were performed at different scanning speeds (e.g., 10 Hz for 10 μm *x–y* scanning line result in 1 μm/s linear velocity for unidirectional movement of the tip) and applying different normal forces. The normal force range was set to 0–300 nN by taking into account the maximum strength of the cantilever used. During LFM analysis, AFM signals such as topographic data, error signal, and horizontal force were also recorded. The studies were carried out at 25°C on the Peltier-element temperature-controlled AFM stage. For homogeneous surfaces with average roughness, local changes in micro-scale friction can sometimes be high and may be due to the distribution of elevations on the surface rather than the local surface slope (Bhushan & Ruan, 1994). In these height differences, while the friction increases in the direction of ascending, the friction force decreases in the direction of descending. For this reason, the horizontal bending coefficient was calibrated using the Si (100) surface according to the literature (Bhushan & Ruan, 1994) (Ogletree, Carpick, & Salmeron, 1996).

3 | RESULTS AND DISCUSSION

3.1 | Characterization of polymer surfaces in terms of topographic, and particle distribution

Topography images of PP samples show the typical structure of linear polymers (please refer to the Figure S1a–g). It is seen from the orientation of the particles that the crystal structures were oriented during the extrusion process. It can be said that PPs have a very smooth surface in topographic images. R_{pv} (maximum height difference between surface structures) and RMS roughness (R_q) values were taken into consideration in the surface roughness analysis performed for PPs. While the R_{pv} value gives the coarse height difference of the material that changes during processing, the RMS roughness value gives the height difference formed by the crystal structures on the material (or small structures such as pigment, if available). Average grain sizes were 20 nm for P1, 70 nm for P2, 35 nm for P3, 80 nm for P4, 110 nm for P5, 105 nm for P6, and 50 nm for P7 (please refer to Table S1).

According to the grain analysis results, the average grain area of P1 crystals consisted of grains with about 1 μm^2, especially 0.5 μm^2 or less. Grains with a surface area of 0.5μm^2 and less constituted more than 50% of the total grains. The average volumes of the grains were less than 0.05 μm^3 and have a single distribution. As a result of the particle analysis of P2, 3 different sized grain distribution was observed. The surface area had a grain distribution of around 0.4 μm^2, there were also some grains with high surface areas around 1.5 and 1.7 μm^2. The grain volume of P2 was around 0.04 μm^3. For P3, on the other hand, grain area and volume distribution centered at 0.4 μm^2 and 0.01 μm^3, respectively. Although there were grain formations in the particle distribution with an area of 1.8 μm^2, the general distribution was consistent with other PP samples. P4 was a low-density polymer used in this study, and its topography has shown that the surface contains larger grains than P1. It was found that P4 crystallized to form larger grains during the recycling process, and the average grain size on the surface after extrusion was nearly four times larger than P1. Grain analyzes of P4, on the other hand, gave a particle area distribution centered at 0.4 μm^2 and a volume distribution at around 0.02–0.01 μm^3. The surface area ratio was 2.03% since P4 was rougher than pigment-free P1. For P5, RMS roughness was found as 110 nm and it is one of the polymers with the highest grain size among the PPs used in the study. Besides, due to this large-grained structure, the polymer with the highest surface area ratio was P5 with 4.28%. The grain surface areas for P5 had two size distributions centered at 0.4 and 0.8 μm^2. Grains of P5 were observed in three different centered size distributions by volume. The volume of the majority of grains was 0.04 μm^3, while the other distribution in the region of 0.08 μm^3. P6 exhibits a structure similar to P5 in terms of topographic analysis. P6 grain analysis showed that there are grains with an area distribution of about 0.5 μm^2. However, there were also grains with a 3 μm^2 surface area. This may be an indication that the temperature is rapidly lowered below the glass-transition temperature of this polymer during extrusion, or that sufficient pressure is not applied in the extrusion. In general, volumetric distribution matches other PP samples. The surface area ratio obtained for P6 was 2.59% and was close to P4. Another PP used in the study was a recycled PP that contains carbon black which is intended to use in the production of high-strength pipes. Unlike other PPs, grains in this polymer appear to be small and frequent (48 nm RMS). It can be seen from the topographic image that the particles are relatively directional (see Figure S1). The grain analysis shows that the grains in P7 were approximately uniform and their surface area distribution was centered around 0.2 μm^2, while volume distribution was centered at 0.02 μm^3.

In general, when grains are small (from R_{pv} and grain analysis), the height of the surface formations (from RMS roughness) was also low. Here, while P4 contained a very low amount of pigment, P1 was pigment-free, and also P6 and P7 have had carbon black as additive. The relationship between the R_{pv}-RMS roughness and the total surface area ratio of the material (ratio between theoretical scanned area and the total calculated area including surface formations) is examined in Figure 2a. As can be seen, there is a significant relationship between R_{pv} and RMS values. It is also observed that there is a significant relationship between the surface area ratio and the roughness values.

3.2 | Comparison of mechanical behaviors of polymers

Indentation experiments have been carried out by using the AFM tip as an indenter in the mechanical characterization of the polymers. *F–z* curves were obtained as a result of the indentation tests (see Figure S2, for representative data). The *F–z* curve was linear with a regression coefficient of 0.99 or higher when the deformation was elastic (at the retrace phase). The elastic modulus of the material was calculated from the *F–z* data using the Hertzian contact model for elastic deformation. In the model used, the angle of the conical AFM tip was 40°, and the Poisson coefficient of the material was taken as 0.42 (average value for PP). The compression-elastic modulus of the polymer beads is given in Table 1.

Since macrostructural defects such as voids and cracks in the material are not evaluated during nanoindentation with AFM, the mechanical properties determined here were likely to be higher than macrotests. The uniformity of the material can be observed from the standard deviation values of the measurements. As well known, material properties at the submicron scale are likely to be position-dependent. In some instances, the standard deviation obtained at around 0.09 GPa remains around 10% of the measured value, but this difference was quite high (note that it is 10 times lower for P3).

The relationship between elastic modulus values measured and the average grain volumes and grain perimeter values obtained from the grain analysis of the material were investigated (Figure 2b). An almost inverse proportional elastic modulus correlation with the grain size was obtained. The graphic given in Figure 2b does not contain

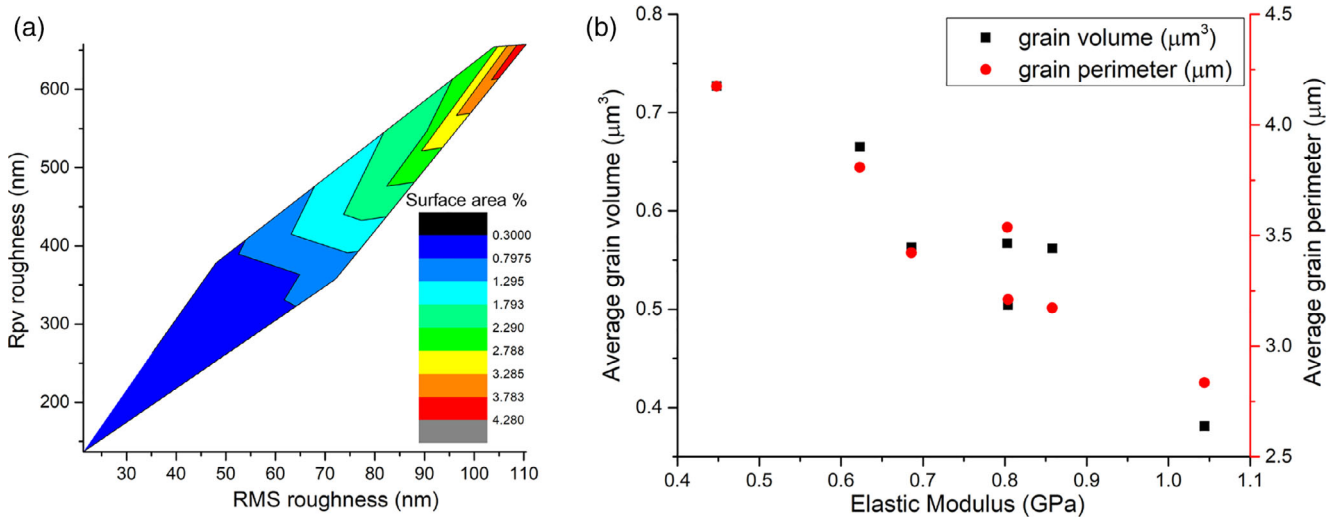

FIGURE 2 (a) The relationship between R_{pv}-RMS roughness and the total surface area ratio of the material (the total calculated surface area/scanned surface area ratio of the material). (b) The relationship between the average grain volume and the grain perimeter value obtained from the particle analysis of the material and the measured elastic modulus

TABLE 1 Compression-elastic modulus obtained from nanoindentation tests

Polymer	Elastic modulus (GPa)	Standard deviation (GPa)
P1	0.858	0.034
P2	0.803	0.089
P3	0.448	0.010
P4	0.804	0.083
P5	0.623	0.062
P6	0.686	0.050
P7	1.044	0.057

error bars for ease of reading. Please refer to Figure S3 for the graphic with the error bar included. There was a clear relationship between the average grain volume (including height data) and average grain perimeter values and the compression-elastic modulus of the material. It was observed that the compression-elastic modulus increased as the crystal size and volume decreased in the PP samples. However, a significant relationship could not be established between the roughness of the material (RMS and R_{pv}) and the elastic modulus.

A different mechanical behavior was obtained in P5, P6, and P7 because the material contains intense pigment such as carbon black and TiO_2. The elastic modulus of high-quality recycled PP material containing carbon black was 1 GPa. Polymer P3, which had the lowest elastic modulus, was a recycled polymer containing red pigment and blended with polyethylene. P1 (high-quality pigment-free recycled PP) and P4 (pigment-containing recycled PP) showed approximately the same elastic behavior. P5 and P6 were recycled PPs that contain different pigments but also have fillers for opacity, and an elastic modulus of around 600 MPa has been obtained.

In general, the modulus values obtained were found to be in agreement with the literature and averaged 750 MPa due to the low crystallinity expected in recycled products (Li et al., 2020).

3.3 | Tribology tests using AFM

In the last step of the study, tribology tests were performed using recycled polymers, and with the AFM tip made of SiC material. For this purpose, in the tribology tests carried out at different tip swiping speeds and different normal loads, the signal resulting from the horizontal bending of the AFM cantilever was calibrated on the Si(100) surface and the friction forces were examined. Contour graphics were drawn from the 512-pixel × 512-pixel data obtained and the actual friction map was created. The friction map is presented in Figure 3 for polymer beads with the lowest (P1) and the highest (P5) friction force, superimposed with topographic images. Friction maps of other polymer beads can be found in Figure S4. Thus, friction force distribution (in nN) was obtained in an area of 5 μm × 5 μm. Mapping can be performed on all samples after AFM-tip calibration. Unfortunately, there is a need for the post-production of the data as there is no such option in the built-in AFM software.

According to the mapping obtained for a certain speed and a normal load during the movement of the AFM tip on the surface, it seems that crystal orientation altered more the friction force (in nN) than the surface shapes. In the friction-map of P1, it is seen that friction increases in the region where the oriented structure is located (in the lower right corner of the figure). Although a friction behavior was observed that follows the surface formation, higher friction values were observed at the regions where the crystal orientation was directly related to the friction force, and where there were large particles compared with other regions (P5, at the right, and bottom left of

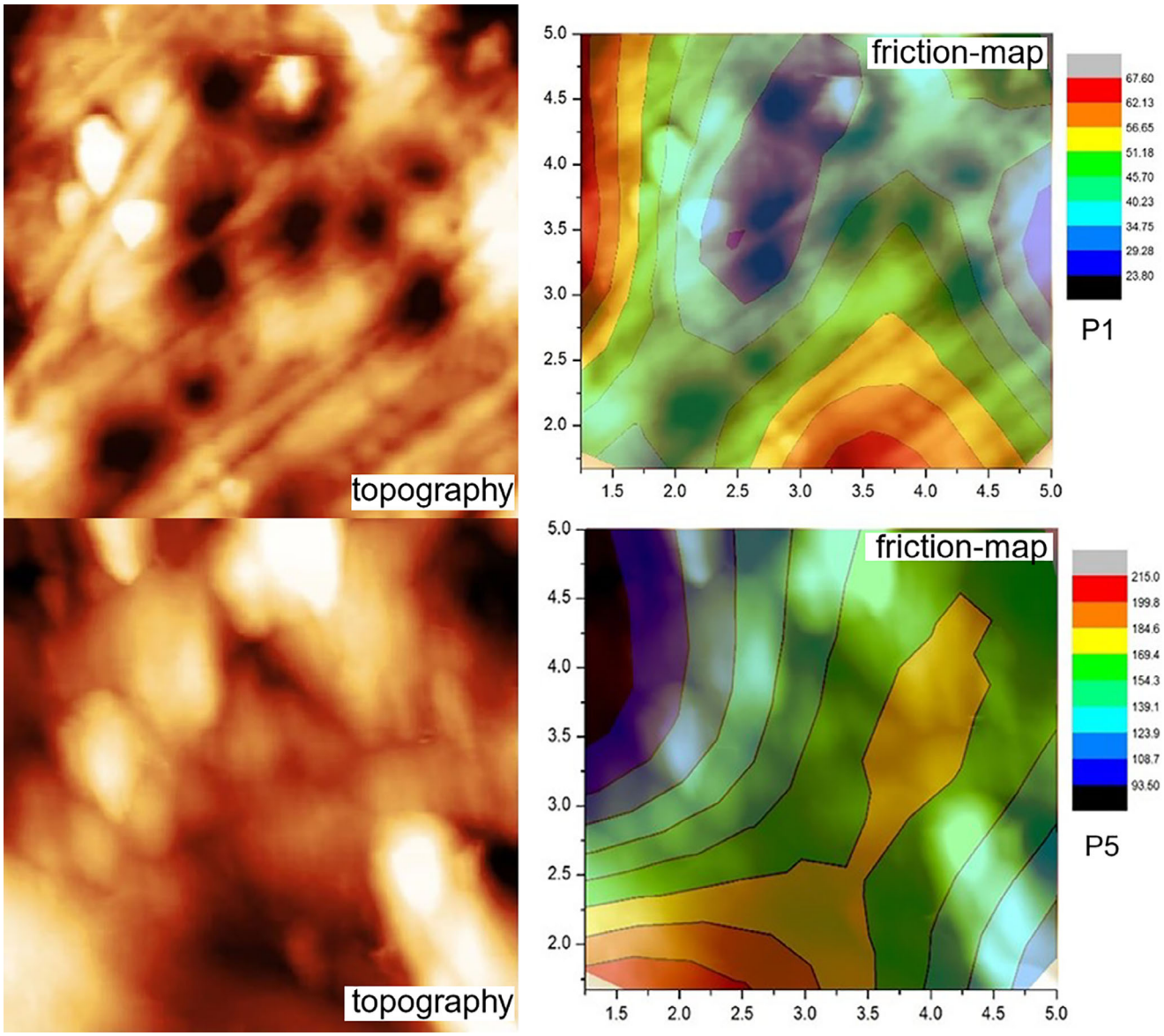

FIGURE 3 Friction-maps obtained from the experiment performed with 20 nN loadings and 5 μm/s scanning speed using polymer beads P1 and P5

the figure). Detailed data for each PP bead sample can be found in Appendix S1.

4 | CONCLUSION

In this study, mechanical properties were determined by using AFM for commercially produced recycled polypropylene, and the sub-micron scale surface properties and the mechanical behavior of the material were investigated. There are many studies on determining the mechanical properties of polymers by nanoindentation. However, the determination of the compression-elastic modulus of recycled polypropylene material was reported first time, by indentation experiments only in the elastic region by applying force at the shallow indentation depth and the elastic deformation regime zone. The effective compression-elastic modulus was calculated by applying the Hertzian model to the obtained *F*–*z* curves. In the roughness analysis of the material, a significant relationship was determined between the maximum height difference (R_{pv}), root-mean-square roughness (RMS), and surface area ratio. No relation could be determined between the surface roughness and the compression-elastic modulus. However, grain analyzes were performed using the device's built-in software, and a significant relationship was determined between the average grain volume and average grain perimeter values, and the compression-elastic modulus. It was determined that the compression-elastic modulus of PP material decreased as the particle volume and perimeter increased. The determined compression-elastic modulus (0.4–1.1 GPa) is a comparable value compared with the value given for pure PP (1.5–2 GPa) in the literature since it is possible to obtain some deterioration in the materials' mechanical

properties during the recycling process (VanLandingham, Villarrubia, Guthrie, & Meyers, 2001). In this study, as presented in other studies conducted with AFM, the elastic modulus (*E*) values obtained were relative measurements obtained when the average spring constants and ideal tip shapes were calculated. It should also be noted that the Hertz model, in which viscoelastic behavior is not taken into account, was used.

Finally, tribologic properties of the material at different shear rates and tensions have been determined and sample friction maps have been constructed for the polymers. Friction maps obtained by overlapping the friction data determined by the application of the calibration techniques specified in the literature with the topographic images were reported for the first time for recycled PP.

AFM has also proved to be a sensitive and successful equipment for the determination and characterization of the mechanical properties of materials in nanoscale.

ACKNOWLEDGMENTS

The financial supports of the Cumhuriyet University Scientific Research Supporting Department (CUBAP) under grant number M589 was gratefully acknowledged.

DATA AVAILABILITY STATEMENT

The data that support the findings of this study are available from the corresponding author upon reasonable request.

ORCID

Mustafa Oguzhan Caglayan https://orcid.org/0000-0002-7265-1094

REFERENCES

Ago, M., Jakes, J. E., & Rojas, O. J. (2013). Thermomechanical properties of lignin-based electrospun Nanofibers and films reinforced with cellulose Nanocrystals: A dynamic mechanical and Nanoindentation study. *ACS Applied Materials & Interfaces*, *5*(22), 11768–11776. https://doi.org/10.1021/am403451w

Barone, A. C., Salerno, M., Patra, N., Gastaldi, D., Bertarelli, E., Carnelli, D., & Vena, P. (2010). Calibration issues for nanoindentation experiments: Direct atomic force microscopy measurements and indirect methods. *Microscopy Research and Technique*, *73*(10), 996–1004. https://doi.org/10.1002/jemt.20850

Benitez, R., & Toca-herrera, J. L. (2014). Looking at cell mechanics with atomic force microscopy: Experiment and theory. *Microscopy Research and Technique*, *77*(11), 947–958. https://doi.org/10.1002/jemt.22419

Bhushan, B., & Kwak, K. J. (2007). Velocity dependence of nanoscale wear in atomic force microscopy. *Applied Physics Letters*, *91*(16), 163113. https://doi.org/10.1063/1.2800375

Bhushan, B., & Ruan, J.-A. (1994). Atomic-scale friction measurements using friction force microscopy: Part II—Application to magnetic media. *Journal of Tribology*, *116*(2), 389–396. https://doi.org/10.1115/1.2927241

Bilodeau, G. G. (1992). Regular pyramid punch problem. *Journal of Applied Mechanics, Transactions ASME*, *59*(3), 519–523. https://doi.org/10.1115/1.2893754

Bolshakov, A., & Pharr, G. M. (2011). Influences of pileup on the measurement of mechanical properties by load and depth sensing indentation techniques. *Journal of Materials Research*, *13*(4), 1049–1058. https://doi.org/10.1557/JMR.1998.0146

Butt, H.-J., Cappella, B., & Kappl, M. (2005). Force measurements with the atomic force microscope: Technique, interpretation and applications. *Surface Science Reports*, *59*(1), 1–152. https://doi.org/10.1016/j.surfrep.2005.08.003

Cao, Y., Allameh, S., Nankivil, D., Sethiaraj, S., Otiti, T., & Soboyejo, W. (2006). Nanoindentation measurements of the mechanical properties of polycrystalline au and Ag thin films on silicon substrates: Effects of grain size and film thickness. *Materials Science and Engineering: A*, *427*(1), 232–240. https://doi.org/10.1016/j.msea.2006.04.080

Cappella, B., & Dietler, G. (1999). Force-distance curves by atomic force microscopy. *Surface Science Reports*, *34*(1), 1–104. https://doi.org/10.1016/S0167-5729(99)00003-5

Cappella, B., & Silbernagl, D. (2008). Nanomechanical properties of polymer thin films measured by force–distance curves. *Thin Solid Films*, *516*(8), 1952–1960. https://doi.org/10.1016/j.tsf.2007.09.042

Cárdenas-Pérez, S., Chanona-Pérez, J. J., Méndez-Méndez, J. V., Arzate-Vázquez, I., Hernández-Varela, J. D., & Vera, N. G. (2019). Recent advances in atomic force microscopy for assessing the nanomechanical properties of food materials. *Trends in Food Science & Technology*, *87*, 59–72. https://doi.org/10.1016/j.tifs.2018.04.011

Chakraborty, H., Sinha, A., Mukherjee, N., Ray, D., & Protim Chattopadhyay, P. (2013). A study on nanoindentation and tribological behaviour of multifunctional ZnO/PMMA nanocomposite. *Materials Letters*, *93*, 137–140. https://doi.org/10.1016/j.matlet.2012.11.075

Chen, D., Cui, X., & Chen, H. (2021). Dual-composite drag-reduction surface based on the multilayered structure and mechanical properties of tuna skin. *Microscopy Research and Technique*, *84*, 1862–1872. https://doi.org/10.1002/jemt.23743

Davies, P., Sohier, L., Cognard, J. Y., Bourmaud, A., Choqueuse, D., Rinnert, E., & Créac'hcadec, R. (2009). Influence of adhesive bond line thickness on joint strength. *International Journal of Adhesion and Adhesives*, *29*(7), 724–736. https://doi.org/10.1016/j.ijadhadh.2009.03.002

Dominguez, J. A., Bittencourt, B., Michel, M., Sabino, N., Gomes, J. C., & Gomes, O. M. M. (2012). Ultrastructural evaluation of enamel after dental bleaching associated with fluoride. *Microscopy Research and Technique*, *75*(8), 1093–1098. https://doi.org/10.1002/jemt.22035

Francius, G., Hemmerlé, J., Ohayon, J., Schaaf, P., Voegel, J.-C., Picart, C., & Senger, B. (2006). Effect of crosslinking on the elasticity of polyelectrolyte multilayer films measured by colloidal probe AFM. *Microscopy Research and Technique*, *69*(2), 84–92. https://doi.org/10.1002/jemt.20275

Frisbie, C. D., Rozsnyai, L. F., Noy, A., Wrighton, M. S., & Lieber, C. M. (1994). Functional group imaging by chemical force microscopy. *Science*, *265*(5181), 2071–2074. https://doi.org/10.1126/science.265.5181.2071

Gao, S.-L., & Mäder, E. (2002). Characterisation of interphase nanoscale property variations in glass fibre reinforced polypropylene and epoxy resin composites. *Composites Part A: Applied Science and Manufacturing*, *33*(4), 559–576. https://doi.org/10.1016/S1359-835X(01)00134-8

García, R., & Pérez, R. (2002). Dynamic atomic force microscopy methods. *Surface Science Reports*, *47*(6), 197–301. https://doi.org/10.1016/S0167-5729(02)00077-8

Godehardt, R., Lebek, W., Adhikari, R., Rosenthal, M., Martin, C., Frangov, S., & Michler, G. H. (2004). Optimum topographical and morphological information in AFM tapping mode investigation of multicomponent polyethylene. *European Polymer Journal*, *40*(5), 917–926. https://doi.org/10.1016/j.eurpolymj.2004.01.034

Greenwood, J. A., & Johnson, K. L. (2006). Oscillatory loading of a viscoelastic adhesive contact. *Journal of Colloid and Interface Science*, *296*(1), 284–291. https://doi.org/10.1016/j.jcis.2005.08.069

Griepentrog, M., Krämer, G., & Cappella, B. (2013). Comparison of nanoindentation and AFM methods for the determination of mechanical properties of polymers. *Polymer Testing*, *32*(3), 455–460. https://doi.org/10.1016/j.polymertesting.2013.01.011

Hardiman, M., Vaughan, T. J., & McCarthy, C. T. (2015). Fibrous composite matrix characterisation using nanoindentation: The effect of fibre constraint and the evolution from bulk to in-situ matrix properties. *Composites Part A: Applied Science and Manufacturing*, *68*, 296–303. https://doi.org/10.1016/j.compositesa.2014.09.022

Hardiman, M., Vaughan, T. J., & McCarthy, C. T. (2016). The effects of pile-up, viscoelasticity and hydrostatic stress on polymer matrix nanoindentation. *Polymer Testing*, *52*, 157–166. https://doi.org/10.1016/j.polymertesting.2016.04.003

Hertz, H. (1882). Ueber die Berührung fester elastischer Körper, *1882*(92), 156–171. https://doi.org/10.1515/crll.1882.92.156

Hoffmann, R., Baratoff, A., Hug, H. J., Hidber, H. R., Löhneysen, H. v., & Güntherodt, H. J. (2007). Mechanical manifestations of rare atomic jumps in dynamic force microscopy. *Nanotechnology*, *18*(39), 395503. https://doi.org/10.1088/0957-4484/18/39/395503

Jandt, K. D. (1998). Developments and perspectives of scanning probe microscopy (SPM) on organic materials systems. *Materials Science and Engineering R: Reports*, *21*(5), 221–295. https://doi.org/10.1016/S0927-796X(97)00012-0

Jin, T., Niu, X., Xiao, G., Wang, Z., Zhou, Z., Yuan, G., & Shu, X. (2015). Effects of experimental variables on PMMA nano-indentation measurements. *Polymer Testing*, *41*, 1–6. https://doi.org/10.1016/j.polymertesting.2014.09.015

Karapanagiotis, I., Evans, D. F., & Gerberich, W. W. (2002). Dynamics of the leveling process of nanoindentation induced defects on thin polystyrene films. *Polymer*, *43*(4), 1343–1348. https://doi.org/10.1016/S0032-3861(01)00688-7

Kawasaki, M., Nobuchi, T., Nakafushi, Y., Nose, M., Shibata, M., Li, P., & Shiojiri, M. (2017). Structural observations and biomechanical measurements of clarinet reeds made from *Arundo donax*. *Microscopy Research and Technique*, *80*(8), 959–968. https://doi.org/10.1002/jemt.22889

Kim, J.-H., Yeon, S.-C., Jeon, Y.-K., Kim, J.-G., & Kim, Y.-H. (2003). Nanoindentation method for the measurement of the Poisson's ratio of MEMS thin films. *Sensors and Actuators A: Physical*, *108*(1), 20–27. https://doi.org/10.1016/j.sna.2003.07.001

King, J. A., Klimek, D. R., Miskioglu, I., & Odegard, G. M. (2013). Mechanical properties of graphene nanoplatelet/epoxy composites. *Journal of Applied Polymer Science*, *128*(6), 4217–4223. https://doi.org/10.1002/app.38645

Kotomin, S. V., Chang, I. T., Sancaktar, E., & Yarikov, D. (2014). The tribology and micromechanics of polystyrene-montmorillonite nanocomposites. *Mechanics of Composite Materials*, *49*(6), 651–658. https://doi.org/10.1007/s11029-013-9381-z

Lee, S.-H., Wang, S., Pharr, G. M., & Xu, H. (2007). Evaluation of interphase properties in a cellulose fiber-reinforced polypropylene composite by nanoindentation and finite element analysis. *Composites Part A: Applied Science and Manufacturing*, *38*(6), 1517–1524. https://doi.org/10.1016/j.compositesa.2007.01.007

Li, J., Zhu, Z., Li, T., Peng, X., Jiang, S., & Turng, L.-S. (2020). Quantification of the Young's modulus for polypropylene: Influence of initial crystallinity and service temperature. *Journal of Applied Polymer Science*, *137*(16), 48581. https://doi.org/10.1002/app.48581

Li, L., Guo, C., Xu, S., Li, X., & Han, C. (2017). Morphology and nanoindentation properties of mouthparts in Cyrtotrachelus longimanus (Coleoptera: Curculionidae). *Microscopy Research and Technique*, *80*(7), 704–711. https://doi.org/10.1002/jemt.22855

Li, X., & Guo, C. (2019). Microstructure and material properties of hind wings of a bamboo weevil Cyrtotrachelus buqueti (Coleoptera: Curculionidae). *Microscopy Research and Technique*, *82*(7), 1102–1113. https://doi.org/10.1002/jemt.23258

Loubet, J. L., Oliver, W. C., & Lucas, B. N. (2000). Measurement of the loss tangent of low-density polyethylene with a nanoindentation technique. *Journal of Materials Research*, *15*(5), 1195–1198. https://doi.org/10.1557/JMR.2000.0169

Magonov, S. N., Elings, V., & Whangbo, M. H. (1997). Phase imaging and stiffness in tapping-mode atomic force microscopy. *Surface Science*, *375*(2), L385–L391. https://doi.org/10.1016/S0039-6028(96)01591-9

Mallikarjunachari, G., & Ghosh, P. (2016). Analysis of strength and response of polymer nano thin film interfaces applying nanoindentation and nanoscratch techniques. *Polymer*, *90*, 53–66. https://doi.org/10.1016/j.polymer.2016.02.042

Morozov, I. A. (2021). Atomic force microscopy nanoindentation kinetics and subsurface visualization of soft inhomogeneous polymer. *Microscopy Research and Technique*, *84*, 1959–1966. https://doi.org/10.1002/jemt.23751

Nagasaki, R., Ishikawa, R., Ito, S., Saito, T., & Iijima, M. (2021). Effects of polishing with paste containing surface pre-reacted glass-ionomer fillers on enamel remineralization after orthodontic bracket debonding. *Microscopy Research and Technique*, *84*(2), 171–179. https://doi.org/10.1002/jemt.23575

Narayanan, V. (1995). A review of: "Mechanical properties of polymers and composites" by Lawrence E. Nielsen and Robert F. Landel. *Materials and Manufacturing Processes*, *10*(4), 856–857. https://doi.org/10.1080/10426919508935076

Ogasawara, N., Chiba, N., & Chen, X. (2005). Representative strain of indentation analysis. *Journal of Materials Research*, *20*(8), 2225–2234. https://doi.org/10.1557/JMR.2005.0280

Ogletree, D. F., Carpick, R. W., & Salmeron, M. (1996). Calibration of frictional forces in atomic force microscopy. *Review of Scientific Instruments*, *67*(9), 3298–3306. https://doi.org/10.1063/1.1147411

Oliver, W. C. (1992). An improved technique for determining hardness and elastic modulus using load and displacement sensing indentation experiments. *Journal of Materials Research*, *7*(6), 1564–1583. https://doi.org/10.1557/JMR.1992.1564

Oliver, W. C., & Pharr, G. M. (2011). Measurement of hardness and elastic modulus by instrumented indentation: Advances in understanding and refinements to methodology. *Journal of Materials Research*, *19*(1), 3–20. https://doi.org/10.1557/jmr.2004.19.1.3

Oyen, M. L. (2015). Nanoindentation of hydrated materials and tissues. *Current Opinion in Solid State and Materials Science*, *19*(6), 317–323. https://doi.org/10.1016/j.cossms.2015.03.001

Park, B. D., Frihart, C. R., Yu, Y., & Singh, A. P. (2013). Hardness evaluation of cured urea-formaldehyde resins with different formaldehyde/urea mole ratios using nanoindentation method. *European Polymer Journal*, *49*(10), 3089–3094. https://doi.org/10.1016/j.eurpolymj.2013.06.013

Pelegri, A. A., & Huang, X. (2008). Nanoindentation on soft film/hard substrate and hard film/soft substrate material systems with finite element analysis. *Composites Science and Technology*, *68*(1), 147–155. https://doi.org/10.1016/j.compscitech.2007.05.033

Rodríguez, J., Garrido-Maneiro, M. A., Poza, P., & Gómez-del Río, M. T. (2006). Determination of mechanical properties of aluminium matrix composites constituents. *Materials Science and Engineering: A*, *437*(2), 406–412. https://doi.org/10.1016/j.msea.2006.07.118

Sader, J. E., Chon, J. W. M., & Mulvaney, P. (1999). Calibration of rectangular atomic force microscope cantilevers. *Review of Scientific Instruments*, *70*(10), 3967–3969. https://doi.org/10.1063/1.1150021

Salerno, M., Dante, S., Patra, N., & Diaspro, A. (2010). AFM measurement of the stiffness of layers of agarose gel patterned with polylysine. *Microscopy Research and Technique*, *73*(10), 982–990. https://doi.org/10.1002/jemt.20838

Samadi-Dooki, A., Malekmotiei, L., & Voyiadjis, G. Z. (2016). Characterizing shear transformation zones in polycarbonate using nanoindentation. *Polymer*, *82*, 238–245. https://doi.org/10.1016/j.polymer.2015.11.049

Sarialioglu Gungor, A., & Donmez, N. (2021). Dentin erosion preventive effects of various plant extracts: An in vitro atomic force microscopy, scanning electron microscopy, and nanoindentation study. *Microscopy*

Research and Technique, *84*(5), 1042–1052. https://doi.org/10.1002/jemt.23665

Song, J., Thurber, C. M., Kobayashi, S., Baker, A. M., Macosko, C. W., & Silvis, H. C. (2012). Blends of polyolefin/PMMA for improved scratch resistance, adhesion and compatibility. *Polymer*, *53*(16), 3636–3641. https://doi.org/10.1016/j.polymer.2012.05.057

Torres-Torres, D., Torres, J. A., & García-García, A. (2019). Finite element simulation based-on atomic force microscopy and nanoindentation for spruce wood microstructure analysis. *Microscopy Research and Technique*, *82*(5), 507–516. https://doi.org/10.1002/jemt.23194

VanLandingham, M. (2018). The effect of instrumental uncertainties on AFM indentation measurements. *Microscopy Today*, *5*(10), 12–15. https://doi.org/10.1017/S1551929500060697

VanLandingham, M. R., Villarrubia, J. S., Guthrie, W. F., & Meyers, G. F. (2001). Nanoindentation of polymers: An overview. *Macromolecular Symposia*, *167*(1), 15–44. https://doi.org/10.1002/1521-3900(200103)167:1<15::aid-masy15>3.0.co;2-t

Vincent, B., & Ramesh, B. (2015). Comparison of ASTM plastic and composite standards on mechanical properties of GFRP composites. *International Journal of Applied Engineering Research*, *10*, 686–688.

Vlad-Cristea, M., Riedl, B., Blanchet, P., & Jimenez-Pique, E. (2012). Nanocharacterization techniques for investigating the durability of wood coatings. *European Polymer Journal*, *48*(3), 441–453. https://doi.org/10.1016/j.eurpolymj.2011.12.002

Wang, X., Deng, Y., Wang, S., Min, C., Meng, Y., Pham, T., & Ying, Y. (2014). Evaluation of the effects of compression combined with heat treatment by nanoindentation (NI) of poplar cell walls, *68*, 167–173. https://doi.org/10.1515/hf-2013-0084

Wang, X., Li, Y., Wang, S., Deng, Y., Xing, D., & He, S. (2015). Investigating the nanomechanical behavior of thermosetting polymers using high-temperature nanoindentation. *European Polymer Journal*, *70*, 360–370. https://doi.org/10.1016/j.eurpolymj.2015.07.037

Weber, A., Iturri, J., Benitez, R., & Toca-Herrera, J. L. (2019). Measuring biomaterials mechanics with atomic force microscopy. 1. Influence of the loading rate and applied force (pyramidal tips). *Microscopy Research and Technique*, *82*(9), 1392–1400. https://doi.org/10.1002/jemt.23291

Withers, J. R., & Aston, D. E. (2006). Nanomechanical measurements with AFM in the elastic limit. *Advances in Colloid and Interface Science*, *120*, 57–67. https://doi.org/10.1016/j.cis.2006.03.002

Wood, C. D., Chen, L., Burkhart, C., Putz, K. W., Torkelson, J. M., & Brinson, L. C. (2015). Measuring interphase stiffening effects in styrene-based polymeric thin films. *Polymer*, *75*, 161–167. https://doi.org/10.1016/j.polymer.2015.08.033

Wornyo, E., Gall, K., Yang, F., & King, W. (2007). Nanoindentation of shape memory polymer networks. *Polymer*, *48*(11), 3213–3225. https://doi.org/10.1016/j.polymer.2007.03.029

Yang, Y., Xiao, X., Peng, Y., Yang, C., Wu, S., Liu, Y., … Jiang, H. (2019). The comparison between force volume and peakforce quantitative nanomechanical mode of atomic force microscope in detecting cell's mechanical properties. *Microscopy Research and Technique*, *82*(11), 1843–1851. https://doi.org/10.1002/jemt.23351

Young, T. J., Crocker, L. E., Broughton, W. R., Ogin, S. L., & Smith, P. A. (2013). Observations on interphase characterisation in polymer composites by nano-scale indentation using AFM and FEA. *Composites Part A: Applied Science and Manufacturing*, *50*, 39–43. https://doi.org/10.1016/j.compositesa.2013.03.014

Yu, Y., Wang, H., Lu, F., Tian, G., & Lin, J. (2014). Bamboo fibers for composite applications: A mechanical and morphological investigation. *Journal of Materials Science*, *49*(6), 2559–2566. https://doi.org/10.1007/s10853-013-7951-z

Zhang, T.-Y., & Xu, W.-H. (2011). Surface effects on Nanoindentation. *Journal of Materials Research*, *17*(7), 1715–1720. https://doi.org/10.1557/JMR.2002.0254

Zheng, Y., Guo, C., Li, L., & Ma, Y. (2019). Morphology and mechanical properties of the dorsal bony plates in the Chinese sturgeon (*Acipenser sinensis*). *Microscopy Research and Technique*, *82*(7), 1083–1091. https://doi.org/10.1002/jemt.23256

Zhou, J., & Komvopoulos, K. (2006). Surface and interface viscoelastic behaviors of thin polymer films investigated by nanoindentation. *Journal of Applied Physics*, *100*(11), 114329. https://doi.org/10.1063/1.2398797

Zhou, X., Jiang, Z., Wang, H., & Yu, R. (2008). Investigation on methods for dealing with pile-up errors in evaluating the mechanical properties of thin metal films at sub-micron scale on hard substrates by nanoindentation technique. *Materials Science and Engineering: A*, *488*(1), 318–332. https://doi.org/10.1016/j.msea.2008.01.020

SUPPORTING INFORMATION

Additional supporting information may be found in the online version of the article at the publisher's website.

How to cite this article: Koç, M. M., & Caglayan, M. O. (2022). Mechanical test and friction-mapping on recycled polypropylene beads using atomic force microscopy. *Microscopy Research and Technique*, *85*(2), 460–468. https://doi.org/10.1002/jemt.23919